Rev. Roum. Sci. Techn.– Électrotechn. et Énerg.
Vol. **66**, *2*, pp. 125–130, Bucarest, 2021

Électronique et transmission de l'information

LINEAR QUADRATIC CONTROLLER FOR TWO-INTERLEAVED BOOST CONVERTER ASSOCIATED WITH PEMFC EMULATOR

AMAR BENAISSA[1], BOUALAGA RABHI[2], MOHAMED FOUAD BENKHORIS[3], LAID ZELLOUMA[4]

Key words: Proton exchange membrane fuel cell (PEMFC), Emulator, Fuzzy logic control, Linear quadratic regulator (LQR), Dc-dc converter, Interleaved boost.

The high cost of fuel cells is the main reason to think of an alternative such as a fuel cell emulator. The emulator must be able to reproduce the nonlinear output voltage-current characteristic fuel cell (FC). This paper then proposes a possible solution for emulating a PEMFC system using a dc/dc buck converter. The converter-based system allows the behavior of fuel cell to be easily emulated and can be used in laboratory as a low-cost system for design and experimental purposes. The structure of the interleaved boost has been applied in view of the advantages such as the reduction of the current ripple delivered by the PEMFC and the reduction of the stresses on the semiconductors since each converter carries 1 / *N* of the current delivered by the PEMFC. Also, in this paper a linear quadratic regulator (LQR) is used to regulate the output voltage of the interleaved boost dc-dc converter. The performance of this controller has been tested under different disturbances using the MATLAB / Simulink simulation package. Simulation results show that the proposed control strategy offers good performances versus load variation, and reference voltage variation.

1. INTRODUCTION

The proton exchange membrane fuel cell (PEMFC) is currently being studied as a power source for various applications such as transportation and uninterruptible power supplies [1–5]. Fuel cell systems are characterized by high costs and complex auxiliary devices. For this reason, a fuel cell emulator can be used as an economical alternative for the development and testing of a fuel cell power conditioning system. In this paper, a dc/dc buck converter is appropriately controlled to accurately describe the *VI* characteristic of a fuel cell. The topologies of the converter have to meet some challenges such as low current / voltage ripples and reliability. The parallel connection of the switched converters or specifically the interleaving approach meets the above requirements with better power extensibility characteristics compared to conventional [6–8]. In the literature, control techniques range from proportional-derivative-integral (PID) control [9, 10] and hysteresis control to sliding mode [6] and repetitive control. They also range from the model predictive control and the fuzzy logic [10] to artificial neural network control and linear quadratic regulator (LQR) control. Although PI regulators are the most common for dc/dc converter control, however, adequate transient performance can not be guaranteed with PI controllers [10]. The LQR regulator ensures the stability of the converter over a wide operating range [10]. It is used to give the best possible performance with respect to some given measure of performance; namely a quadratic function is composed of a state vector and a control input. Simulation results shows that the proposed control strategy offers good performances versus load variation, and reference voltage variation. The work is organized as follows. Section 2 briefly shows a model of a PEM based on the simulation of the relationship between the output voltage and the partial pressures of hydrogen, oxygen and water. Thus, in Section 3, the block diagram of the PEMFC emulator is described and presented. After converter modeling in Section 4, a linear quadratic controller (LQR) is designed for two interleaved boost dc/dc converter in Section 5, results and discussions are presented in Section 6. Finally, the conclusions are summarized.

2. PEM FUEL CELL MODEL

To simulate a PEM, a model of a solid oxide fuel cell (SOFC) presented by Padulles *et al.* [1] was modified. This model is based on the simulation of the relationship between the output voltage and the partial pressures of hydrogen, oxygen and water [2, 3].

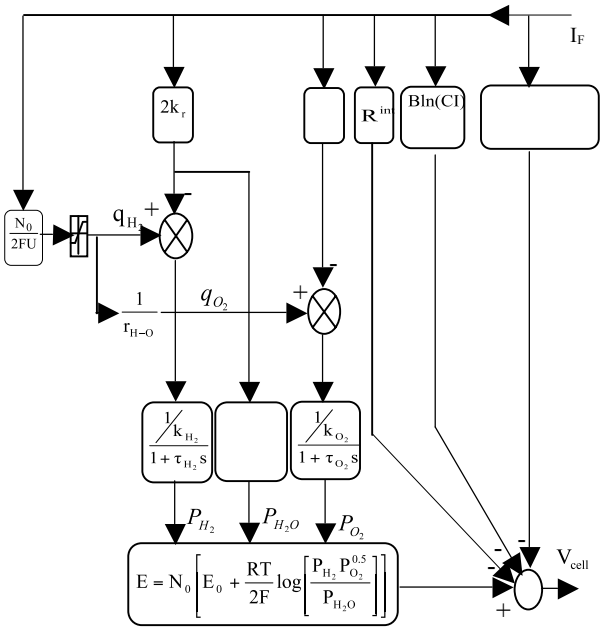

Fig. 1 – PEM fuel cell model.

[1] LAADI Laboratory, University of Djelfa, Algeria, E-mail: benaissa_am@yahoo.fr
[2] LMSE Laboratory, University of Biskra, Algeria
[3] IREENA-CRTT Laboratory, University of Nantes,Saint Nazaire, 44600, France
[4] LEVRES Laboratory, University of El-Oued, Algeria

The detailed model of the PEM fuel cell shown in Fig. 1, describe the fuel cell stack voltage under loaded condition given by subtracts the various loss from the open circuit dc voltage and expressed as:

$$V_{cell} = E - V_{ohmic} - V_{activation} - V_{concentration}, \quad (1)$$

where

$$E = N_0 \left[E_0 + \frac{RT}{2F} \log \left[\frac{P_{H_2} P_{O_2}^{0.5}}{P_{H_2O}} \right] \right]. \quad (2)$$

E is called the Nernst voltage or reversible voltage that exist at no load condition for a given temperature and pressure.

$$V_{ohmic} = I_{FC}.R^{int}. \quad (3)$$

V_{ohmic} is the resistive voltage loss due to the resistance of non-ideal electrodes and connections and the resistance to proton flow in the PEM.

$$V_{activation} = B \ln(CI). \quad (4)$$

$V_{activation}$ is the voltage loss corresponding to the activation losses due to the rate of reaction taking place on the surface of the electrodes, and

$$V_{concentration} = -cln(1 - \frac{I}{I_{Lim}}). \quad (5)$$

$V_{concentration}$ is the voltage loss corresponding to the voltage change due to mass transport losses. The PEMFC model parameters are presented in Table 1.

Table 1

Parameters of the PEMFC model

Activation current constant (C)	0.4959 [A^{-1}]
Activation voltage constant (B)	0.02956 [V]
Concentration voltage constant (c)	0.06[V]
Faraday's constant (F)	96484600 [$Ckmol^{-1}$]
Hydrogen time constant (τH2)	3.37[s]
Hydrogen valve constant (KH2)	4.22 x 10^{-5} [kmol (s atm)$^{-1}$]
Hydrogen-oxygen flow ratio (τH-O)	1.168
Kr constant = N_0 /4F	2.5911 x 10^{-9} [kmol (s A)$^{-1}$]
N_0 load cell voltage (E_0)	0.8 [V]
Number of cells (N_0)	1
Oxygen time constant (τO2)	6.74[s]
Oxygen valve constant (K O2)	2.11 x 10^{-5} [kmol (s atm)$^{-1}$]
FC internal resistance (R^{int})	0.01778 Ω
FC absolute temperature (T)	343[K]
Universal gas constant (R)	8314.47 [J (kmol K)$^{-1}$]
Utilization factor (U)	0.8
Water time constant (τH2O)	18.418 [s]
Water valve constant (KH2O)	7.716 x 10^{-6} [kmol (s atm)$^{-1}$]

The simulated characteristics of PEM fuel cell stack voltage for the fixed values of input fuel pressures for single cell is presented in Fig. 2. It can be seen that at low current level, the ohmic loss becomes less significant and the increase in output voltage is mainly due to activity of slowness of chemical reactions. So this region is also called active polarization. At very high current density the voltage fall down significantly because of the reduction of gas exchange efficiency.

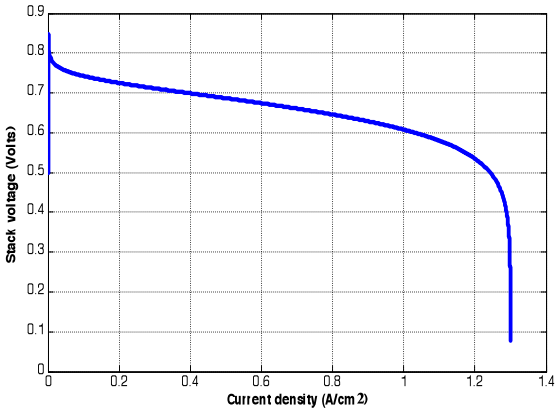

Fig. 2 – Characteristics curve of PEM fuel cell single stack..

This is mainly due to over flooding of water in catalyst and this region is also called concentration polarization. Intermediate between the active region and concentrations region there is a linear slope which is mainly due to internal resistance offered by various components of the fuel cell. This region is generally called as ohmic region [2, 3].

3. EMULATOR SYSTEM DESCRIPTION

Figure 3 shows the PEMFC emulator. The model block of the PEMFC system is modeled in Simulink Matlab. The input of the model is the load current I_{FC} required by the load. Besides V_{ref} is the value of the reference voltage corresponding to the current I_{FC} according to the characteristic *V-I* of the PEMFC. The controller processes the signal V_{ref} and U_s and gives the corrected value of the duty cycle to the dc-dc converter.

In Fig. 3, Buck converter used for emulation is shown, where the value of parasitic resistance R_1 and R_2 are 0.01 and 0.02 ohm respectively. The value of inductor and capacitor are 5e-3 H and 8000e-6 F. The entire model of the PEMFC system shown in Figure 1, as well as the control system of the dc-dc converter has been simulated in Matalb.

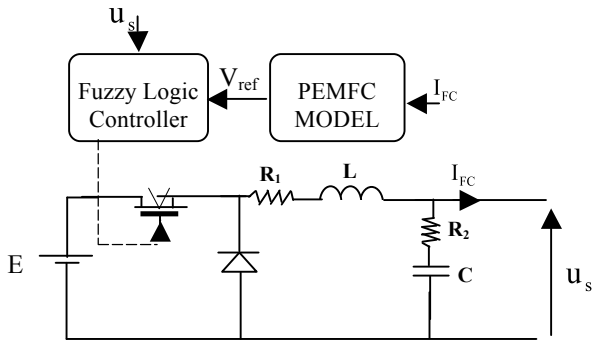

Fig. 3 – Buck converter used as emulator .

3. 1 FUZZY LOGIC CONTROLLER

In this application, the fuzzy control algorithm is implemented to track V_{ref} delivered by the fuel cell model based on voltage error e(k) processing and its variation Δe(k) . In the design of a fuzzy control system, the formulation of its rule set plays a key role in improving the system performance. The rule table contains 49 rules as shown in Table 2, where (LP, MP, SP, ZE, LN, MN, and SN) are linguistic codes (LP: large positive; MP: medium positive; SP: small positive; ZE: zero; LN: large negative; MN: medium negative; SN: small negative). The fuzzy control rules as given in Table 2 was done with Mamdani Methods and the defuzzification was done with the centre of gravity method to calculate the output of Fuzzy Logic Controller FLC (duty cycle). The output voltage is compared with the reference voltage and generated error signal. The output of FLC is compared with a saw tooth reference signal to generate a PWM signal which drives the switching MOSFET.

Table 2

Fuzzy control rule table

Δe	e						
	NL	NM	NS	ZE	PS	PM	PL
NL	NL	NL	NL	NL	NM	NS	ZE
NM	NL	NL	NL	NM	NS	ZE	PS
NS	NL	NL	NM	NS	ZE	PS	PM
ZE	NL	NM	NS	ZE	PS	PM	PL
PS	NM	NS	ZE	PS	PM	PL	PL
PM	NS	ZE	PS	PM	PL	PL	PL
PL	NL	NM	NS	ZE	PS	PM	PL

4. BOOST CONVERTER MODEL

Consider the boost converter given in Fig. 4. The following expression defines the variable states chosen to describe the model

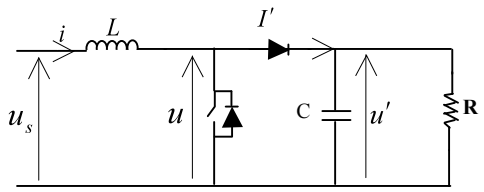

Fig. 4 – Boost converter.

$$\begin{cases} \dfrac{\mathrm{d}i}{\mathrm{d}t} = \dfrac{u_s}{L} - \dfrac{u}{L} \\ \dfrac{\mathrm{d}u'}{\mathrm{d}t} = -\dfrac{u'}{cR} + \dfrac{I'}{c} \end{cases}. \tag{6}$$

The mean value of u and I' can be described as follow:

$$u = u'(1-\alpha). \tag{7}$$

$$I' = i(1-\alpha). \tag{8}$$

Where α is duty cycle of the boost converter, the state space average model of the boost converter is:

$$\begin{cases} \dfrac{\mathrm{d}i}{\mathrm{d}t} = -\dfrac{1-\alpha}{L}u' + \dfrac{u_s}{L} \\ \dfrac{\mathrm{d}u'}{\mathrm{d}t} = \dfrac{1-\alpha}{c}i - \dfrac{u'}{cR} \end{cases}. \tag{9}$$

The linearization of the model around the following equilibrium point:

$$x_0 = \begin{bmatrix} \dfrac{u_s}{R(1-\alpha_0)^2} \\ \dfrac{u_s}{1-\alpha_0} \end{bmatrix}. \tag{10}$$

Based on this linearization, the small-signal model can be described as follows:

$$\begin{bmatrix} \dot{\hat{i}} \\ \dot{\hat{u}}' \end{bmatrix} = \begin{bmatrix} 0 & -\dfrac{1}{L}(1-\alpha_0) \\ \dfrac{1}{c}(1-\alpha_0) & -\dfrac{1}{cR} \end{bmatrix} \begin{bmatrix} \hat{i} \\ \hat{u}' \end{bmatrix} + \begin{bmatrix} \dfrac{u_s}{L(1-\alpha_0)} \\ -\dfrac{u_s}{Rc(1-\alpha_0)^2} \end{bmatrix} \hat{\alpha}. \tag{11}$$

4. 1 LINEAR QUADRATIC CONTROLLER

The model of the controllers used in the computer simulation is shown in Fig. 5. The (LQR) controller has the objective of tracking the discrete reference *u'ref (k)* in each sample instant. The state variables used in the (LQR) are the variation of the inductor current *î(k)* defined as the difference between the measured current *i(k)* and the equilibrium point $i_o(k)$, the variation of the output voltage *û'(k)* defined as the difference between the measured output voltage *u'(k)* and the equilibrium point $u'_o(k)$ and the integrated tracking error. Each state variable has weighting K_i tuned according to the plant parameters. The control system shown in Fig. 5 is therefore proposed.

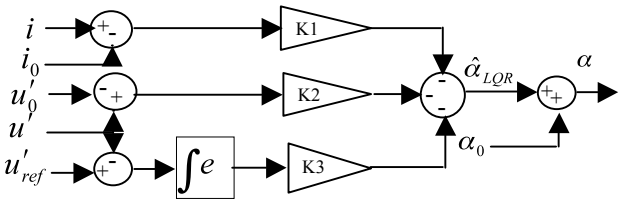

Fig. 5 – Block diagram of the LQR controller.

The model in eq. (11) is then augmented with an additional state variable in order to control the output voltage *u'*.The new state variable is defined as:

$$\dot{\left[\int e\right]} = e = u'_{ref} - u' = -\hat{u}'. \tag{12}$$

The augmented small signal can be written:

$$\begin{bmatrix} \dot{\hat{i}} \\ \dot{\hat{u}}' \\ \dot{\int e} \end{bmatrix} = \begin{bmatrix} 0 & -\dfrac{1}{L}(1-\alpha_0) & 0 \\ \dfrac{1-\alpha_0}{c} & -\dfrac{1}{cR} & 0 \\ 0 & -1 & 0 \end{bmatrix} \begin{bmatrix} \hat{i} \\ \hat{u}' \\ \int e \end{bmatrix} + \begin{bmatrix} \dfrac{u_s}{L(1-\alpha_0)} \\ -\dfrac{u_s}{Rc(1-\alpha_0)^2} \\ 0 \end{bmatrix} \hat{\alpha}. \tag{13}$$

Or

$$\dot{x} = Ax + Bu, y = Cx\,, \tag{14}$$

where

$$C = \begin{bmatrix} 0 & 1 & 0 \end{bmatrix}. \tag{15}$$

Then, a discrete time model of the plant and sample time T_S is given by:

$$x(k+1) = A_d x(k) + B_d u(k), y(k) = C_d x(k)\,, \tag{16}$$

where

$$A_d = I + T_S A\,. \tag{17}$$

$$B_d = (\int_0^T \mathrm{e}^{A\tau}\mathrm{d}\tau)B\,. \tag{18}$$

Then, in the proposed system, the state vector $x(k)$ is defined as:

$$x(k) = \begin{bmatrix} \hat{i}(k) & \hat{u}'(k) & \int e(k) \end{bmatrix}^{\mathrm{T}}. \tag{19}$$

and the LQR control signal is given by

$$\hat{\alpha}_{LQR}(k) = -Kx(k)\,. \tag{20}$$

The optimal gains K_1, K_2, K_3 of the control law in eq. (20) are those that minimize the following cost function:

$$J = \frac{1}{2}\sum_{k=0}^{\infty}\left\{ x^{\mathrm{T}}(k)Qx(k) + \hat{\alpha}^{\mathrm{T}}(k)R_u\hat{\alpha}(k) \right\}, \tag{21}$$

where Q and R_u in eq. (21) are chosen as positive definite matrices that set the weighting of each state and of the control signal. The K gains can be obtained through the evaluating the Riccati equations as follows:

$$S(k) = A_d{}^{\mathrm{T}} S(k+1)A_d + Q - \left[B_d{}^{\mathrm{T}} S(k+1)A_d\right]^{\mathrm{T}} \times \left[R_u + B_d{}^{\mathrm{T}} S(k+1)B_d\right]^{-1}\left[B_d{}^{\mathrm{T}} S(k+1)A_d\right], \tag{22}$$

$$K(k) = R_u{}^{-1}B_d{}^{\mathrm{T}}\left(A_d{}^{\mathrm{T}}\right)^{-1}\left(S(k) - Q\right). \tag{23}$$

A good flexibility in the design of the controller is provided by the selection of Q and R_u matrixes.

5. INTERLEAVED BOOST CONVERTER

The two structures in parallel are shown in Fig. 6, where the inductors are independent of one another. Each converter conducts for αT, the control of k_1 is out of phase with k_2 by $T/2$. If we suppose that the switch k_1 starts at the initial instant, we have as start instant for k_2: $T/2$.

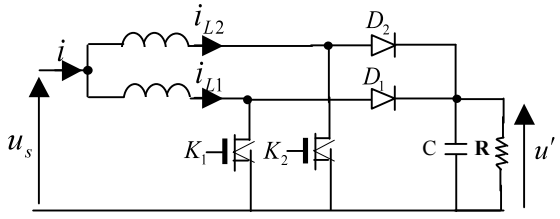

Fig. 6 – Two interleaved boost converter.

6. RESULTS AND DISCUSSIONS

Based on the control schemes for each entity, we deduce the overall scheme of the proposed control system. Figure 7 shows the proposed control system used in simulation.
Thus, the proposed system is composed of a buck converter designed to emulate the PEMFC, associated with two interleaved boost converter as shown in Fig. 7.

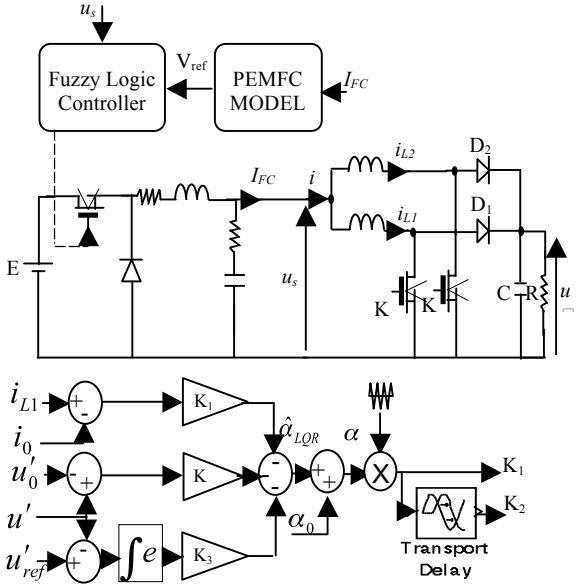

Fig. 7 – Overall scheme of the proposed control system.

6. 1 SIMULATION AND RESULTS OF THE EMULATOR OF THE PEMFC

The parameters of the buck converter are presented in Table 3.

Table 3

Parameters of the buck converter

Dc input voltage	15 V
Switching frequency	10 kHz
Inductor	5 mH
Capacitance	8 mF
parasitic resistance r_1	0.01 Ω
parasitic resistance r_2	0.02 Ω

The result of the simulation in Fig. 8, shows the comparison of the reference *V-I* Characteristic of the PEMFC model and the Characteristic *V-I* of the dc/dc buck converter. It is remarkable that the reference characteristic *V-I* of the PEMFC model has been reproduced perfectly by dc/dc converter.

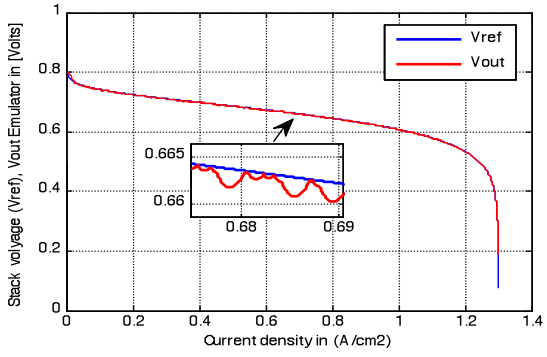

Fig. 8 – Characteristics curve of PEM fuel cell single stack.

6. 2 SIMULATION AND RESULTS OF TWO-INTERLEAVED BOOST CONVERTER ASSOCIATED WITH PEMFC EMULATOR

The typical interleaved converter with the parameters in the Table 4, associated with an emulator of a PEMFC will be studied in closed loop under the LQR controller presented in Fig. 7. The performance of the LQR controller will be checked by different scenarios and tested in the following subsections

Table 4
Interleaved converter parameters

Parameters	L_1	L_2	C	F	R
Value	5 mH	5 mH	0.09 mF	20 kHz	50 Ω

The model parameters of the PEMFC shown in Figure 7, are given in Table 1. A linear quadratic controller is used for the output voltage control, which has the objective of tracking the discrete reference $u'_{ref}(k)$ in each sample instant. The LQR controller parameters are presented in Table 5.

Table 5
LQR parameters

Parameters	Sample time	States weightings	Control
Value	$50e^{-8}$s	Q=diag [0.2 0.2 0.1]	Ru=10
Parameters	Optimal gains for V_{ref}= 70V	Optimal gains for V_{ref}= 80 V	Carrier frequency
Value	K_1=0.6146 K_2=0.0906 K_3= –2.45e^{-4}	K_1=0.6125 K_2=0.0871 K_3= –2.30e^{-4}	Fc = 20 KHz

6. 2 .1 VARIABLE REFERENCE OUTPUT VOLTAGE

Figure 9 illustrates the continuous state evolution of the 2IBC associated with an emulator of a PEMFC in closed loop for a variable reference output voltage. The series of changes in reference voltage is converted to stack current to calculate the corresponding reference fuel cell voltage. The reference PEMFC voltage is tracked by a fuzzy logic controller. The transient and steady state response of the system using LQR controller has been found to be excellent as shown in Fig. 9, it is obvious that the increase in reference output voltage as shown in Fig. 9 (a), increases the FC current as shown in Fig. 9 (c), which results in decreased PEMFC output voltage as shown in Fig. 10. The structure of the interleaved boost contributes successfully to the reduction of the current ripple delivered by the PEMFC. One can remark that the fuel cell current I_{FC} has a minimal ripple in different phases of output reference voltage variations as shown in Fig. 9(b) and 9(c).

Figure 11 shows the duty cycle evolution, it is evident that an increase in reference output voltage increases the value of the duty cycle, which in turn increases output current of the fuel cell I_{FC}. Figure 12 shows the state commutation of the switch K_1, One can remark that the frequency is clearly 20 kHz.

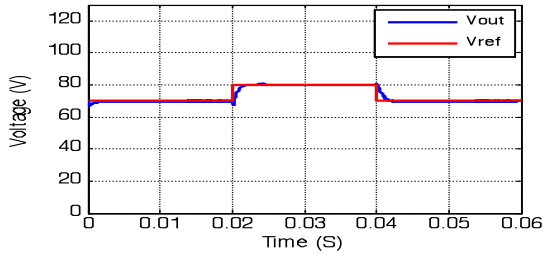

(a) Output voltage evolution.

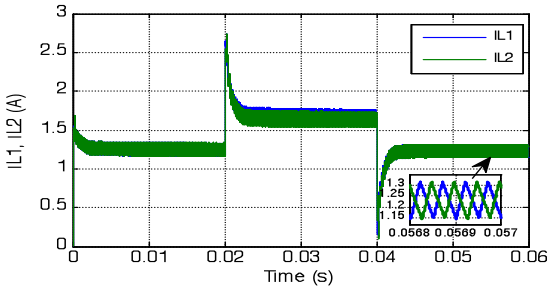

(b) Inductors currents evolution.

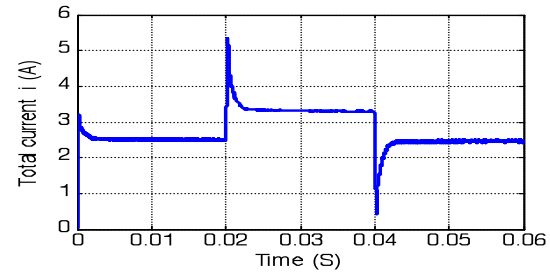

(c) Total current delivered by the PEMFC.

Fig. 9 – State evolution of the 2IBC associated with fuel cell source under a variable reference voltage.

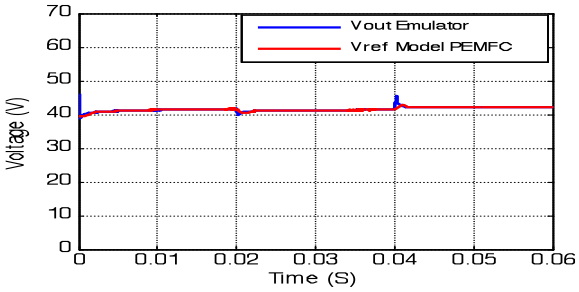

Fig. 10 – PEMFC voltage under a series of reference voltage variation.

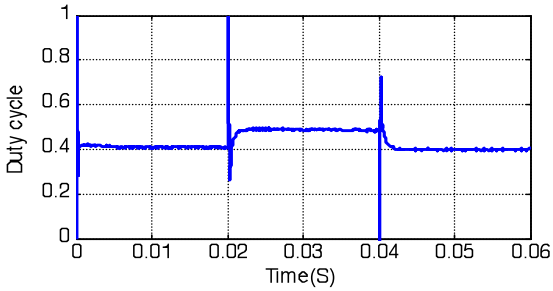

Fig. 11 – Duty cycle evolution under reference voltage variation.

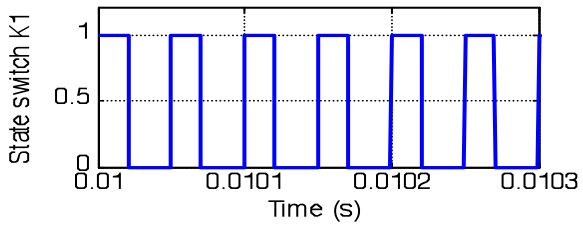

Fig. 12 – State Switch commutation.

6. 2 .2 VARIABLE LOAD RESISTANCE

Figure 13 shows the obtained results for a desired output voltage V_{ref} = 80 V under a variable load resistance. The latter is decreased from 40 Ω to 26.6 Ω at 0.02 s and increased from 26.6 Ω to 40 Ω at 0.04 s.

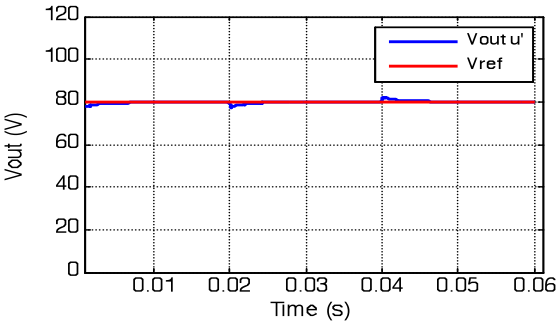

Fig.13 – Output voltage evolution

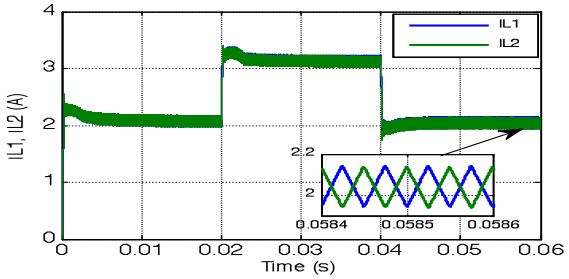

Fig.14 – Inductors currents evolution.

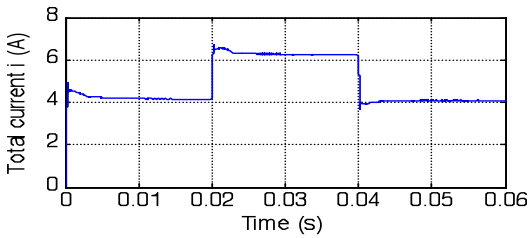

Fig.15 – Total current delivered by the PEMFC.

The transient and steady state response of the system using LQR controller has been found to be excellent as shown in Fig. 13, it is obvious that the decrease in load resistance increases the FC current as shown in Fig. 15.

The structure of the interleaved boost contributes successfully to the reduction of the undulation of the current delivered by the PEMFC. One can remark that the fuel cell current I_{FC} has a minimal ripple in different phases of load resistance variations as shown in Fig. 14 and 15. Figure 16 shows the duty cycle evolution, it is evident that the value of the duty cycle is unaffected by load resistance variation.

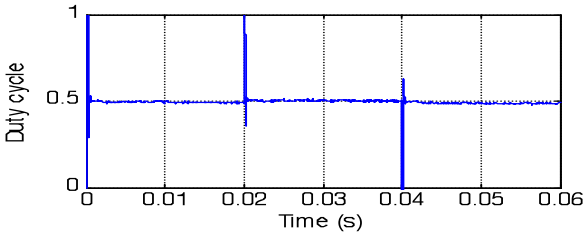

Fig. 16 – Duty cycle evolution under a variable load resistance.

7. CONCLUSION

In this paper a possible solution to emulate a PEMFC system by using a dc/dc buck converter is discussed. The reference characteristic *V-I* of the PEMFC model has been reproduced perfectly by dc/dc buck converter. The structure of the interleaved boost allows the reduction of the undulation of the current delivered by the PEMFC, and the reduction of the stresses on the semiconductors. Also, this paper introduces a technique based on linear quadratic controller (LQR) designed for two interleaved boost dc/dc converter operating in continuous conduction mode. After converter modeling and controller design, the simulations have been done by Matlab/Simulink software. The performances of the LQR controller are tested by introducing changes in desired output voltages. As a final conclusion, the obtained results show that, the proposed control strategy offers good performances versus load variation, and reference voltage variation.

Received on July 27, 2019

REFERENCES

1. J. Padulles, G.W. Ault, J.R. McDonald, *An integrated SOFC plant dynamic model for power systems simulation*, J. POWER Sources **86**, pp. 495–500, (2000).
2. Goce L. Arsov, *Improved Parametric Pspice Model of a PEM Fuel Cell* 11th International Conference on optimization of Electrical and Electronics Equipment, May 2008, pp. 203–208.
3. K.W.E. Cheng, D. Sutanto, Y.L. Ho, K.K. Law, *Exploring the Power Conditioning System for Fuel Cell* 32nd IEEE Annual Power Electronics Specialists Conference, 2001, pp. 2197–2202.
4. M.Y. El-Sharkh, A. Rahman, M. S. Alam, P.C. Byrne, A.A. Sakla, T. Thoma,. *Proton exchange membrane fuel cell dynamic model for residential use,* IEEE Trans. Energy Conversion, June (2003).
5. Fatima Zohra Zerhouni, Mohamed Telidjane, *Branchement Direct D'une Pile A Combustible A Membrane Echangeuse De Protons A Une Charge Et Modelisation,* Rev. Roum. Sci. Techn. Électrotechn. et Énerg., **60**, *4*, pp. 387–396 (2015).
6. L. Zellouma , B. Rabhi, A. Krama, A. Benaissa, M.F. Benkhoris, *Simulation And Real Time Implementation Of Three Phase Four Wire Shunt Active Power Filter Based On Sliding Mode Controller,* Rev. Roum. Sci. Techn.– Électrotechn. et Énerg., **63**, *1*, pp. 77–82 (2018).
7. C. Wang, *Investigation on interleaved boost converters and applications,* Phd thesis, Virginia Polytechnic Institute and State University, USA (2009).
8. Constantin Marin, Dan Selisteanu, Dorin Sendrescu, *Nonlinear identification and control of DC-DC Converter based on heterogeneous approach,* Rev. Roum. Sci. Techn. Électrotechn. et Énerg., **56**, *3*, pp. 325–335 (2011).
9. A. Krama, L. Zellouma, B. Rabhi, *Anti-windup proportional integral strategy for Shunt active power filter interfaced by photovoltaic System using technique of direct power control,* Rev. Roum. Sci. Techn.– Electrotechn. et Energ., **62**, *3,* pp. 252–257 (2017).
10. G. Liping, J. Y. Hung, and R. M. Nelms, *Evaluation of DSP-Based PID and Fuzzy Controllers for DC–DC Converters,* IEEE Transactions on Industrial Electronics, **56**, pp. 2237–2248 (2009).